

Photodegradation of Orange II under Visible Light Using Cu–Ni/TiO₂: Influence of Cu:Ni Mass Composition, Preparation, and Calcination Temperature

Nadia Riaz,^{*,†,||} Fai Kait Chong,^{*,‡} Zakaria B. Man,[†] M. Saqib Khan,^{†,||} and Binay K. Dutta[§]

[†]Chemical Engineering Department, and [‡]Fundamental & Applied Sciences Department, Universiti Teknologi PETRONAS, 31750 Tronoh, Malaysia

[§]West Bengal Pollution Control Board, 10A, Block III, Salt Lake, Kolkata 700 098, India

^{||}COMSATS Institute of Information Technology, Tobe Camp, University Road, 22060, Abbottabad, Pakistan

S Supporting Information

ABSTRACT: Bimetallic Cu–Ni/TiO₂ photocatalysts were prepared at different temperatures with varying Cu:Ni mass compositions. The photocatalysts were further calcined at selected temperatures. Characterization procedures were carried out on the photocatalysts to understand the correlation between the photocatalytic activity and the physicochemical and morphological properties. Results from the XRD, FESEM-EDX mapping, and HRTEM analyses were in favor of the metal particles existing in the form of well-dispersed oxides on TiO₂ surface. The surface area of the photocatalysts was almost similar to the bare TiO₂ (~43 m² g⁻¹) except for 1Cu:9Ni-200-b observed with a higher surface area (53.8 m² g⁻¹) as compared to other photocatalysts. The photocatalyst performance of the bimetallic system is promising as compared to bare TiO₂ and the monometallic photocatalysts. Results for photodegradation studies showed that 1:9 Cu:Ni mass composition was observed with 100% Orange II removal as compared to other Cu:Ni mass compositions. The 1Cu:9Ni-200-a photocatalyst prepared at lower temperature (8–10 °C) displayed 100% Orange II decolorization as compared to 1Cu:9Ni-200-b (prepared at higher temperature of 25 °C) with 65.1% dye removal. Although the results from UV–vis spectra showed the disappearance of the visible band (indicating 100% Orange II removal), TOC analysis indicated the presence of organic compounds derived from the dye degradation process. Therefore, longer irradiation time is required to break the chromophore groups in the degradation intermediates to obtain 100% TOC removal.

1. INTRODUCTION

The textile industry is the major contributor responsible for the aquatic ecosystems' pollution due to the generated wastewaters that are known to contain considerable amounts of nonfixed dyes, especially azo dyes, and a huge amount of inorganic salts. It has been estimated that more than 10% of the total dyestuff used in dyeing processes is released into the environment.^{1,2} The World Bank estimates that 17–20% of industrial water pollution comes from textile dyeing and wastewater treatment from industry.

Azo dyes are the largest group of synthetic colorants used in the textile industry³ constituting 60–70% of all dyestuffs produced.⁴ They have one or more azo groups (R₁–N=N–R₂) having aromatic rings mostly substituted by sulfonate group (–SO₃) and hydroxyl group (–OH), etc.^{5,6} These dyes are nonbiodegradable and toxic and at present are abated by some common nondestructive processes.^{7,8} The model azo dye in this study, Orange II as shown in Figure 1, represents more than 15% of the world production of dyes used in the textile manufacturing industry. Orange II is an anionic monoazo textile dye of the acid class. It is resistant to light degradation, action of O₂, and common acids or bases. In wastewater treatment plants, Orange II does not undergo biological degradation.⁹ The high stability of Orange II is useful in textile manufacturing, but a problem arises later due to difficulty in managing its removal.

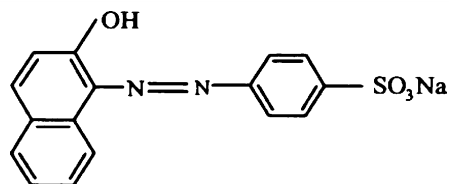


Figure 1. Chemical structure of Orange II.

Treatment of residual dyes has been an important issue of research. Although textile dyes can be disposed via some physical and chemical processes, these methods are usually incomplete and ineffective. Additionally, biological processes exhibited limited efficiency due to xenobiotic and non-biodegradable characteristics of textile dyes. Furthermore, some physical and chemical treatments of dyes can generate secondary pollution resulting from toxic products.¹⁰ Alternatively, photodegradation of dyes has important practical applications because the complete destruction or mineralization of toxic and nonbiodegradable compounds to carbon dioxide and inorganic constituents can be accomplished.¹¹

Received: December 1, 2012

Revised: February 10, 2013

Accepted: February 20, 2013

Published: February 20, 2013

Semiconductor photocatalysis has been investigated extensively for light-stimulated degradation of pollutants, particularly for complete destruction of toxic and nonbiodegradable compounds to carbon dioxide and inorganic constituents.^{8,12–16} The fundamentals of semiconductor photocatalysis and its application to the removal of chemical pollutants have been extensively reviewed.^{8,17–19} Several semiconductors exhibit band gap energies suitable for photocatalytic degradation of contaminants. Among the photocatalysts applied, titanium dioxide is one of the most widely employed photocatalytic semiconducting materials because of the peculiarities of chemical inertness, nonphotocorrosion, low cost, and nontoxicity. Carp et al.¹² cited many references and pointed out that doping semiconductors with various metal ions, composite semiconductors, deposition of group VIII metals, and oxygen reduction catalysts can be employed to enhance photocatalytic efficiency.

The use of Cu and Ni as bimetallic catalyst supported on different semiconductor materials has been reported as the effective method to improve the efficiency of various reactions like carbon dioxide hydrogenation,²⁰ steam reforming of methane,²¹ liquid-phase glycerol hydrogenolysis by formic acid over Ni–Cu/Al₂O₃ catalysts,²² decomposition of methane over Ni–SiO₂ and Ni–Cu–SiO₂ catalysts,²³ and for photocatalytic reduction of nitrate.²⁴ Only a few studies have been reported using Cu, Ni, or Cu–Ni photocatalysts for azo dye degradation like Cu–Zn/TiO₂,²⁵ Ni/TiO₂,²⁶ and Cu–Fe/TiO₂²⁷ for methyl orange degradation, and Cu/TiO₂ for Orange II degradation with 90% color removal in the presence of UVC light and O₂ after 150 min of reaction.²⁸

In our previous studies, Cu–Ni/TiO₂ photocatalysts were prepared employing deposition–precipitation (DP) method.²⁹ The present work deals with the bimetallic TiO₂ photocatalyst preparation via modified co-precipitation method (CP), an effective method to synthesize highly active Cu/TiO₂ photocatalysts reported by Yoong et al.,³⁰ for photocatalytic hydrogen production. The introduction of Cu and Ni was with the intention to reduce the band gap of the photocatalyst for enhanced visible light absorption. The photocatalysts were further characterized using thermogravimetric analysis (TGA), Fourier transform infrared spectroscopy (FTIR), powder X-ray diffraction (XRD), field-emission scanning electron microscopy-energy dispersive X-ray (FESEM-EDX), high-resolution transmission electron microscopy (HRTEM), diffuse reflectance UV visible spectroscopy (DR-UV-vis), point of zero charge (PZC) determination, and surface area analysis employing the Brunauer–Emmet–Teller method (BET).

The objective of this Article was to determine the photoactivity of bimetallic 10 wt % Cu–Ni/TiO₂ prepared with different Cu:Ni mass composition. The effect of preparation and calcination temperatures on the photocatalyst performance was also considered.³¹ The Cu–Ni/TiO₂ bimetallic photocatalysts were investigated for Orange II photodegradation under visible light source, using Orange II as a model azo dye.

2. EXPERIMENTAL DETAILS

2.1. Materials. Copper nitrate trihydrate, Cu(NO₃)₂·3H₂O (Acros brand >98% purity), and nickel nitrate hexahydrate, Ni(NO₃)₂·6H₂O (Acros brand >98% purity), were used as dopant metal salts. Titanium dioxide, TiO₂ (Degussa P25 80% anatase, 20% rutile), was used as a support, which also acts as the semiconductor in photocatalysis. Sodium hydroxide, NaOH

(Merck, 95%), was used as precipitating agent. Glycerol (Systemer, 95% purity) was also used for photocatalysts preparation. Orange II (Acros, pure mono sodium salt) was used as the model azo dye for photocatalytic degradation study. All chemicals were used as received without further purification.

2.2. Preparation of Bimetallic Photocatalyst. A series 10 wt % bimetallic Cu–Ni/TiO₂ photocatalysts with different Cu:Ni mass composition (9:1, 5:5, and 1:9) were prepared using TiO₂ as support via coprecipitation (CP) method. Appropriate amounts of metal salts were dissolved in distilled water, followed by the addition of glycerol in 2:1 glycerol:metal mol ratio.³² TiO₂ was added into the solution with continuous stirring for 1 h prior to precipitation with 0.25 M NaOH. The preparation temperature was maintained in the range from 8 to 10 °C. The final pH was kept at 14, and the mixture was aged for 1 day. The precipitates were filtered and dried in an oven at 75 °C overnight. The raw photocatalysts were ground into a fine powder, kept in an airtight glass bottle, and stored in a desiccator.

The best performing photocatalysts identified from the screening process (100% Orange II removal) were selected for further investigation into the effect of higher preparation temperature on photocatalysts performance. In this case, photocatalysts with 1:9 Cu:Ni mass composition were prepared at 25 °C. The monometallic photocatalysts were also prepared for comparison.

2.3. Pretreatment of Photocatalysts. To estimate suitable calcination temperatures for the raw photocatalysts, thermal gravimetric analyses (TGA) were carried out using a Perkin-Elmer (Pyris 1 TGA) instrument. The raw photocatalysts were weighed using a built-in microbalance attached to the instrument, which automatically read the weight of the sample in the range of 5–10 mg in an aluminum sample cup. The samples were heated from 30 to 800 °C at a heating ramp rate of 20 °C min^{−1} using nitrogen as purging gas at a rate of 20 mL min^{−1}. Results from TGA were reported as thermograms, which are plots of the relative mass (%) of the photocatalysts versus temperature. Denotation for the raw photocatalyst is “xCu:yNi” where x:y is the mass composition of Cu:Ni. On the other hand, denotation for calcined photocatalysts is “xCu:yNi-T” where x:y is the mass composition of Cu:Ni, T is the calcination temperature in °C, and t is the photocatalyst preparation temperature, a = 8–10 °C and b = 25 °C. For example, 1Cu:9Ni-200-a means photocatalysts prepared with 1:9 Cu:Ni mass composition at 8–10 °C and calcined at 200 °C for 1 h duration.

Fourier transform infrared spectroscopy (FTIR) was employed to study the effect of calcination on the type of chemical species present on the photocatalysts. The analyses were conducted using a Shimadzu FTIR-8400S spectrophotometer and scanned from 4000 to 400 cm^{−1}.

2.4. Characterization. To understand the correlation between the photocatalytic activity and physicochemical and/or morphological properties of the Cu–Ni/TiO₂ photocatalysts, characterization was conducted using powder X-ray diffraction (XRD) (Bruker D8 Advance diffractometer), field-emission scanning electron microscopy-energy dispersive X-ray (FESEM-EDX) (Supra55VP), high-resolution transmission electron microscopy HRTEM (Zeiss Libra 200), diffuse reflectance UV visible spectroscopy (DR-UV-vis) (Shimadzu UV3150 NIR), point of zero charge determination (PZC), BET total surface analysis (Micrometrics ASAP 2000), and temperature programmed reduction (TPR) (Thermo Finnigan

TPDRO 1100). The phases present in the photocatalysts were investigated using XRD with Cu K α radiation (40 kV, 40 mA) at 2 θ angles from 10° to 80°, with a scan speed of 4° min⁻¹. The morphology of the photocatalysts such as crystallite particle shape, size, and particle size distribution was analyzed using FESEM and HRTEM. DR-UV-vis measurement was performed using a UV-vis spectrophotometer equipped with an integrating sphere. Reflectance spectra were recorded at 190–800 nm wavelength. DR-UV-vis absorption spectra were recorded as a Kubelka–Munk function, $F(R)$, versus wavelength using a Shimadzu UV3150 NIR spectrophotometer, equipped with integrating sphere. The wavelength ranged from 190 to 800 nm. Barium sulfate (Ba₂SO₄) powder was used as a standard, an internal reference. The band gap energies of the photocatalysts are determined from the extrapolation onto the x -axis of the Tauc plot, which is a plot of $(F(R) \cdot h\nu)^{1/2}$ against $h\nu$. Reflectance spectrum was collected as R-sample/reference and then plotted applying the Kubelka–Munk theory to determine band gap energy.³³ The surface area of photocatalyst was determined using isotherm adsorption of N₂ onto the photocatalyst by applying the Brunauer–Emmet–Teller method. This method is based on the multipoint nitrogen adsorption–desorption principle. The BET surface area of the photocatalysts was determined using a surface analyzer. For each analysis, approximately 0.2–0.3 g of sample was weighed into a sample tube with filler rod inside. Prior to the analysis, each photocatalyst sample was degassed at 130 °C overnight. It is very important to determine the property of the photocatalyst–solution interface especially when the photocatalyst is intended for dye degradation in aqueous solution. PZC (the pH at which the net charge is zero) was determined by the mass titration method reported by Di Paola et al.³⁴ A weighed amount of photocatalyst was mixed with distilled water to give concentrations of 0.1, 1.0, 2.0, 5.0, and 10.0% (w/v). The suspensions were stirred for 24 h to equilibrate the adsorption–desorption processes, after which the pH of the suspensions was determined using a pH meter (TOLEDO 320 pH meter). PZC value was taken at the point where further addition of solids did not produce any significant pH change.

The TPR analyses were conducted to determine the reducibility of the photocatalysts using Thermo Finnigan TPDRO 1100 equipment. Prior to reduction, the sample was pretreated under nitrogen at 110 °C with a flow rate of 20 mL min⁻¹ and ramp rate of 10 °C min⁻¹, and finally holding at 110 °C for 30 min to eliminate moisture before cooling to room temperature. TPR analysis was carried out in 5% H₂ in N₂ with a flow rate of 20 mL min⁻¹. Samples were heated with a ramp rate of 20 °C min⁻¹ from 40 to 500 °C and holding at 800 °C for 10 min. The reduction profile was a plot of hydrogen consumption versus temperature.

2.5. Photocatalytic Degradation Study. Photocatalytic degradation of 50 ppm Orange II was conducted using halogen lamp (500W) as the visible light source at 25 °C with an initial solution pH 6.8. Photocatalyst was weighed and mixed with distilled water and then ultrasonicated for 10 min using an ultrasonicator. Orange II solution then was added to give a final concentration of 50 ppm (with photocatalyst loading 1 g L⁻¹) and total volume of 30 mL. The suspension was stirred using a magnetic stirrer for 2 h in the dark, and later this suspension was illuminated for 1 h using a 500 W halogen lamp as the visible light source at a distance of 25 cm (46.16 W m⁻²). During the dark and light reactions, samples were taken at

certain time intervals to monitor for the degree of Orange II removal.

2.6. Orange II Concentration Monitoring and Mineralization. The Orange II degradation during photoreaction was monitored by measuring the solution absorbance from 400 to 800 nm using a Shimadzu UV-3101 UV/visible spectrophotometer. A calibration curve was obtained beforehand using standard solutions with known Orange II concentrations (1, 10, 20, 30, 50, and 60 ppm). Prior to the absorbance measurement, the reaction samples were centrifuged twice at 3500 rpm for 10 min to remove the suspended photocatalyst. The absorbance peak at 485.0 nm was used as the representative peak for Orange II concentration.^{35,36} The photodecolorization efficiency in terms of % Orange II removal was calculated using eq 1:

$$\text{Orange II removal (\%)} = \left(\frac{C_0 - C}{C_0} \right) \times 100 \quad (1)$$

where C_0 is the initial concentration, while C is the concentration of Orange II at sampling time.

At the end of the reaction, total organic carbon (TOC) analysis was conducted. TOC is defined as the amount of carbon bound in an organic compound, which is an important parameter to assess the organic load of wastewater. Final TOC values (in ppm) and % TOC removal were determined using eq 2.

$$\text{TOC removal (\%)} = \left(\frac{\text{TOC}_0 - \text{TOC}}{\text{TOC}_0} \right) \times 100 \quad (2)$$

Reaction parameters investigated were different Cu:Ni mass composition, photocatalyst preparation temperature, calcination temperatures, and irradiation time. Analyses were also conducted for blank experiments where reactions were carried out using monometallic photocatalysts, without the addition of photocatalyst, and with nonmodified TiO₂.

2.7. High Performance Liquid Chromatography Analysis (HPLC). Orange II photodegradation products were analyzed using high performance liquid chromatography (HPLC Agilent 1100 series) equipped with auto sampler. The analysis was carried out using a Zorbex SB-C18 5 μ m, 150 mm \times 10 mm column with a mobile phase 70:30 aqueous solution of ammonium acetate (20 mM) and acetonitrile at a flow rate of 1 mL min⁻¹, while retention time was 20 min at ambient temperature. The injection volume was 5 μ L, room temperature 22.2 °C, column temperature 26.6 °C, and 117 bar pump pressure. Detector was operated at three different wavelengths: 485, 254, and 215 nm (DAD-UV lamp). Standard solutions were prepared in the eluent with different known concentrations. Some intermediates^{37,38} and products^{39,40} of Orange II photodegradation were used as standards for analysis, and the results were used to determine their compositions during reaction. The standards are benzaldehyde (99.5%, Fluka), benzyl alcohol (Fluka), formaldehyde (Assay \geq 36.5%), formic acid (\geq 98%), oxalic acid (\geq 99.0%, Fluka), propionic acid (\geq 99.8%), sulfanilic acid (\geq 99.0%, Fluka), and 2-naphthol (99%, Aldrich). Calibration curves were obtained for all of the standards with known concentrations.

3. RESULTS AND DISCUSSION

3.1. Pretreatment of Photocatalyst. **3.1.1. Thermogravimetric Analysis.** The thermogram of the raw photocatalyst

1Cu:9Ni is shown in Figure 2. Two decomposition steps were observed from 30 to 170 °C and another from 170 to 500 °C

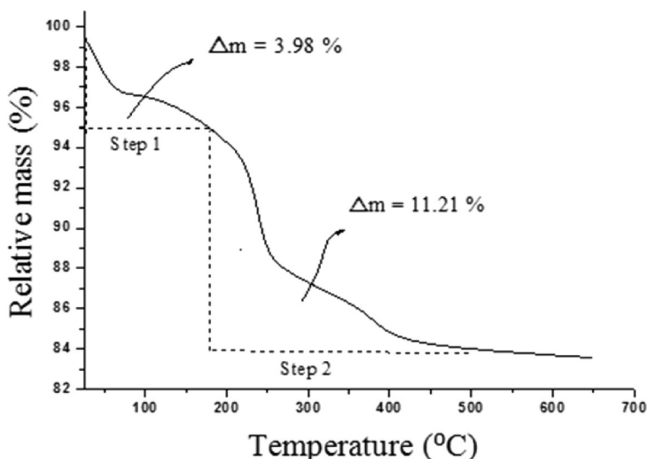
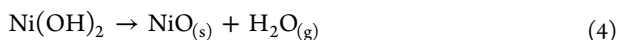
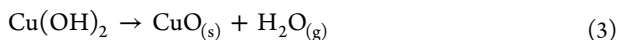


Figure 2. Thermogram of 1Cu:9Ni.

with 3.98% and 11.21% weight loss, respectively. These are attributed to moisture loss and decomposition of $\text{Cu}(\text{OH})_2$ or $\text{Ni}(\text{OH})_2$ to form copper oxide, CuO ,³⁰ or nickel oxide, NiO , respectively. The total weight loss was about 15.19%. Thus, the proposed decomposition steps for the raw photocatalysts are shown in eqs 3 and 4.



Thermograms of the other raw photocatalysts (not shown) with different Cu:Ni mass composition (9:1 and 5:5) are similar to that displayed in Figure 2. On the basis of the thermogram, three calcination temperatures were selected, 180, 200, and 300 °C, for duration of 1 h. The straight horizontal line at 500 °C indicates that thermal stability has been reached and there is no further decomposition.

3.1.2. Fourier Transform Infrared Spectroscopy (FTIR). Figure 3 shows the FTIR spectra of the bare TiO_2 , raw, and calcined photocatalysts. The IR band observed from 400 to 900 cm^{-1} corresponds to the Ti–O stretching vibrations.⁴¹ Several absorption peaks are also observed, mainly 3400 and 1600 cm^{-1} corresponding to O–H stretching and O–H bending,

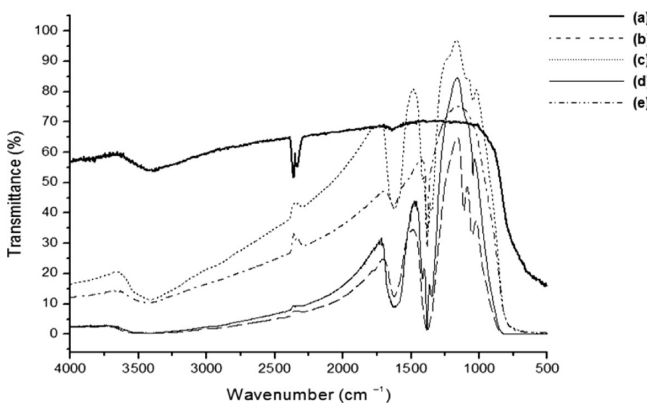


Figure 3. FTIR spectra of (a) bare TiO_2 , (b) 1Cu:9Ni, (c) 1Cu:9Ni-180-a, (d) 1Cu:9Ni-200-a, and (e) 1Cu:9Ni-300-a.

respectively, of physically absorbed moisture. From the FTIR spectra, there was no evidence for the presence of any band at 3635 cm^{-1} representing the absence of Si–OH contamination⁴² during photocatalysts preparation in a glass beaker. The presence of nitrate (NO_3^-) group was observed with a sharp band at 1382 cm^{-1} for the raw and calcined photocatalysts, which is always present when nitrate salts are used as precursors.³³ The FTIR spectra of the other raw photocatalysts (not shown) with different Cu:Ni mass composition (9:1 and 5:5) also displayed peaks similar to those shown in Figure 3.

3.2. Characterization. The photocatalytic behavior of any material is determined by physicochemical and electronic parameters that are difficult to be correlated. The photoactivity derived from a balance of these factors, some of which often play contrasting roles.³⁴ The knowledge of the crystal structure, surface area, porosity, and surface hydroxyl group density is essential to understand the activity of a photocatalyst. In dilute binary oxides, the major component controls the oxide structure, and the dopant surface concentration controls the number of new acid sites.⁴³

3.2.1. Powder X-ray Diffraction (XRD). The XRD patterns of bare TiO_2 , 1Cu:9Ni-200-a, and the monometallic photocatalysts (10Cu:0Ni-200-a, 0Cu:10Ni-200-a) are presented in Figure 4. The XRD patterns for all of the samples are similar

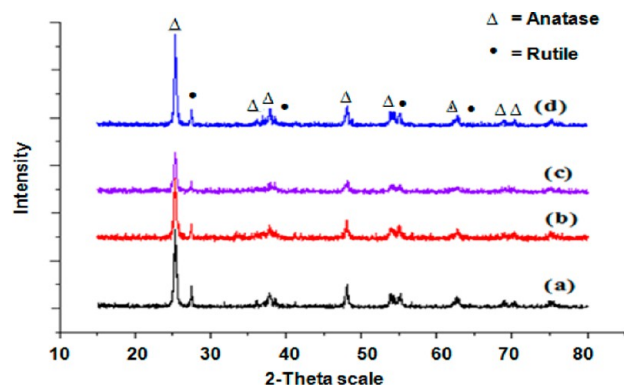


Figure 4. XRD patterns of (a) bare TiO_2 , (b) 1Cu:9Ni-200-a, (c) 10Cu:0Ni-200-a, and (d) 0Cu:10Ni-200-a.

with main peaks at $2\theta = 25.34^\circ$ and 27.46° corresponding to anatase and rutile phases, respectively.^{29,44,45} No phase transition from anatase to rutile was observed for the calcined photocatalysts. Similar patterns were also observed for the other photocatalysts with different Cu:Ni mass composition and calcination temperatures as reported in our previous study.²⁹ The absence of characteristic peaks for Cu and Ni oxides phases may indicate high metallic dispersion^{46–50} or due to the low dopant concentration as reported by Zhu et al.,⁵¹ in which characteristic peaks of metal oxide phase could only be visible when the metal dopant concentration on TiO_2 was above 5 wt %. However, the absence of any metal oxide peaks even at 10 wt % metal loading in this work may indicate very good dispersion of dopant metals Cu, Ni, or mixed Cu–Ni oxide phases onto TiO_2 . This may be due to the use of glycerol during photocatalyst preparation that favored the formation of small metal particles since it has been reported that glycerol prohibited the aggregation of metal particles.⁵²

3.2.2. Photocatalyst Morphology: FESEM and HRTEM. FESEM micrographs of the calcined Cu–Ni/ TiO_2 photocatalysts as compared to bare TiO_2 and the monometallic

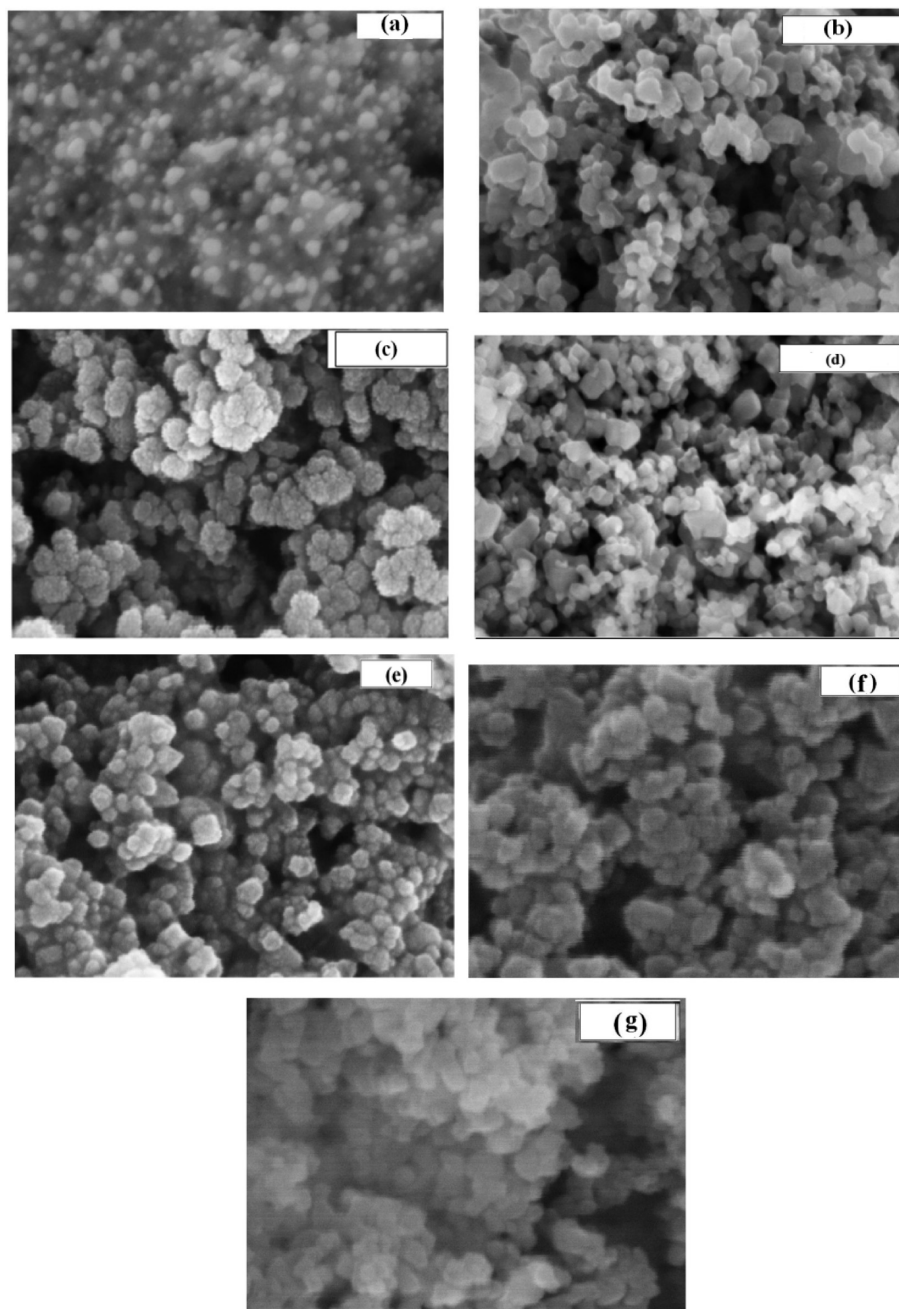


Figure 5. FESEM micrographs at 150 \times magnification of (a) bare TiO₂, (b) 1Cu:9Ni-180-a, (c) 1Cu:9Ni-200-a, (d) 1Cu:9Ni-300-a, (e) 1Cu:9Ni-200-b, (f) 10Cu:0Ni-200-a, and (g) 0Cu:10Ni-200-a.

photocatalysts are displayed in Figure 5. All micrographs displayed irregular-shaped crystallite (11–35 nm) with agglomeration. It can be observed from the EDX-mapping in Figure 6a and b of the photocatalysts that the Cu and Ni dopant metals are uniformly dispersed onto the support. Yoong et al.³⁰ have reported similar agglomeration for Cu/TiO₂ prepared using a similar method. At higher preparation temperature (1Cu:9Ni-200-b), similar morphologies were observed with high agglomeration.

High resolution transmission electron microscopy (HRTEM) was carried out for the detailed analysis of the morphology of the photocatalysts with different Cu:Ni mass compositions. HRTEM images are shown in Figure 7. It can be deduced that the photocatalyst samples consist of very fine crystallite particles (11 $\bar{3}$ 5) with irregular shape. The TiO₂

particles in bare TiO₂ sample tend to stick to each other, which might be due to the high content of surface hydroxyl groups contributing toward the hydrophilic properties.⁵³ The average size for anatase and rutile particles was about 20 nm, which is in good agreement with the FESEM results.

3.2.3. Diffuse Reflectance UV–Visible Spectroscopy (DR–UV–Vis). To determine the band gap energy of the photocatalysts, DR–UV–vis analysis was conducted. The absorption spectrum and DR–UV–visible spectra of bare TiO₂ and Cu–Ni/TiO₂ photocatalysts with different Cu:Ni mass compositions are presented in Figures 8 and 9. Modification with metal can shift the absorption spectrum of TiO₂ into the visible region. The shift in the absorption edge has been observed in the present case indicating higher absorption in the region of 400–800 nm as compared to bare TiO₂. The DR–UV–vis

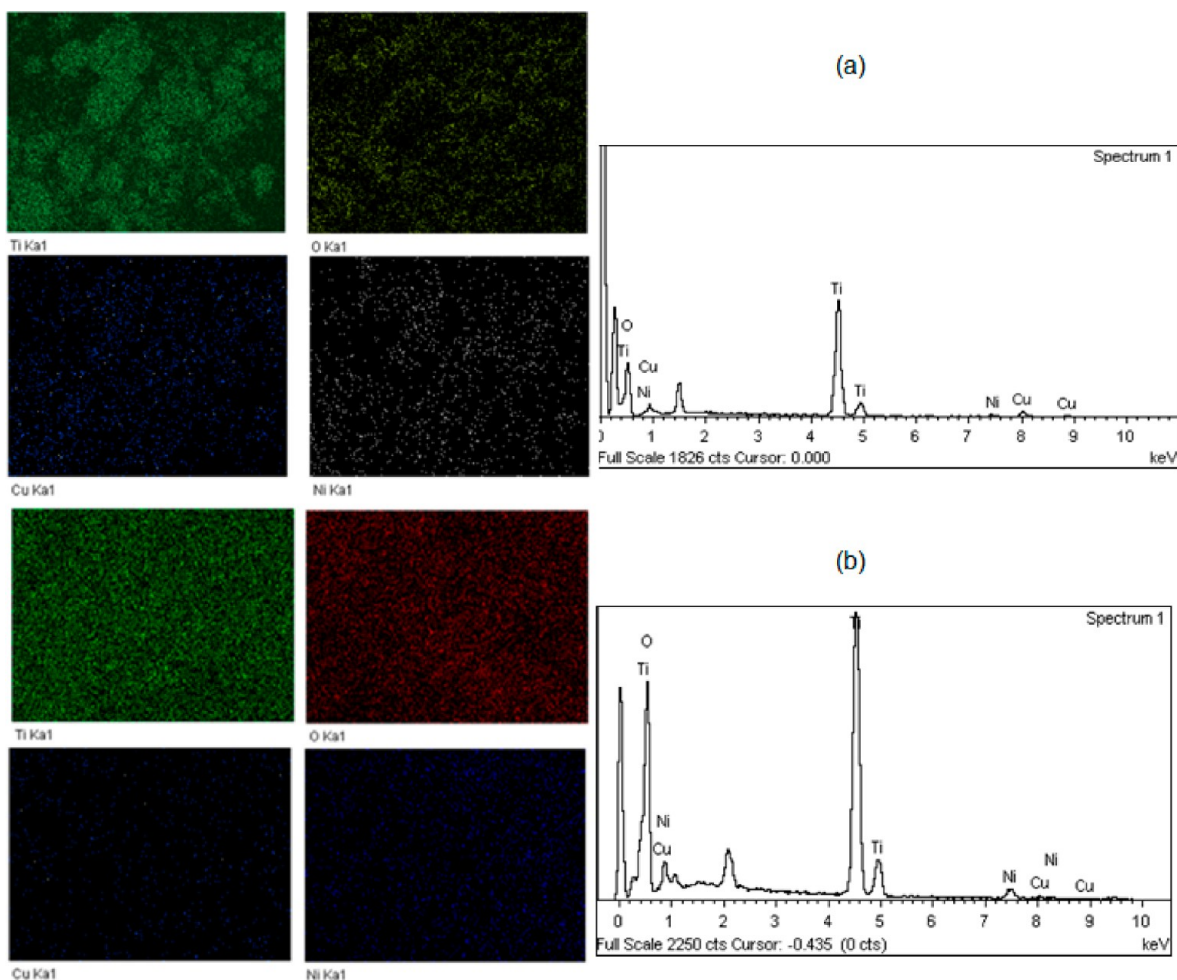


Figure 6. EDX spectra and elemental mapping of (a) 1Cu:9Ni-200-a and (b) 1Cu:9Ni-200-b.

spectrum of bare TiO₂ showed absorption peaks ranging from 190 and 400 nm, similar to that observed by Yoong et al.³⁰ and Riaz et al.²⁹ The absorption at 323 nm is generally related to the electronic excitation from O 2p valence band to Ti 3d conduction band indicating that Ti presents as a tetrahedral Ti⁴⁺ species.⁵⁴ The bulk properties of TiO₂ are as important as the surface properties of TiO₂.⁵⁵ The light absorption properties of TiO₂ modified with Cu–Ni were enhanced significantly. The reason for shift is possibly due to the impurity of energy level as the metals are well dispersed onto the surface of TiO₂ and not incorporated into TiO₂ framework. The band gap energies determined from the Tauc plot, a plot of $(F(R) \cdot h\nu)^{1/2}$ against $h\nu$, for the photocatalysts as compared to bare TiO₂ are presented in Table 1. $F(R)$ is the Kubelka–Munk function derived from reflectance spectra where $F(R) = (1 - R)^2/2R$, and $h\nu$ is the photon energy. The band gap for bare TiO₂ was 3.16 eV. Complete Orange II removal was observed for 1Cu:9Ni-180-a and 1Cu:9Ni-200-a only with band gap at 2.90 and 2.80 eV, respectively. Although 1Cu:9Ni-200-b showed absorbance similar to 1Cu:9Ni-180-a and band gap at 2.90 eV also (overlapping and not clearly visible here), the Orange II removal was 65% only. This indicates that the efficiency of the photocatalysts does not depend only on the band gap value.

3.2.4. The Surface Area of Photocatalyst. All of the photocatalysts displayed Type IV isotherms with hysteresis loops (as in Figure 10), which indicates capillary condensation

in mesoporous adsorbate,⁵⁶ while TiO₂ displayed type III pattern, which is typically ascribed to nonporous products with weak interactions between the adsorbent and the adsorbate. Surface area, pore volume, and pore diameter were higher for Cu–Ni/TiO₂ photocatalysts as compared to bare TiO₂ (Table 1). Surface area is high at lower calcination temperature but decreased with increasing temperature. For 1Cu:9Ni–200-a, surface area is slightly lower (40 m² g⁻¹) as compared to bare TiO₂ (43.1 m² g⁻¹). However, at other calcination temperatures (180 and 300 °C), the photocatalysts displayed higher surface area as compared to bare TiO₂; for 1Cu:9Ni-180-a and 1Cu:9Ni-300-a, the surface area was 50 and 45.8 m²/g, respectively. High metal dispersion on TiO₂ surface was reported when the total surface area of photocatalysts was increased.^{29,57} With reference to pore volume, the results are almost similar at different calcination temperatures, while pore diameter was the highest (30.1 nm) for 1Cu:9Ni-200-a as compared to the photocatalysts calcined at 180 and 200 °C.

The effect of photocatalyst preparation temperature showed that photocatalyst prepared at higher temperature (1Cu:9Ni-200-b) displayed higher surface area (53.8 m²/g), pore volume (0.49 cm³/g), but lower pore diameter (18.4 nm) as compared to that prepared at lower temperature (1Cu:9Ni-200-a) with lower surface area (40 m²/g), lower pore volume (0.30 cm³/g), but higher pore diameter (30.1 nm). There seems to be no clear correlation between these values with the Orange II removal efficiency. However, for photocatalysts with

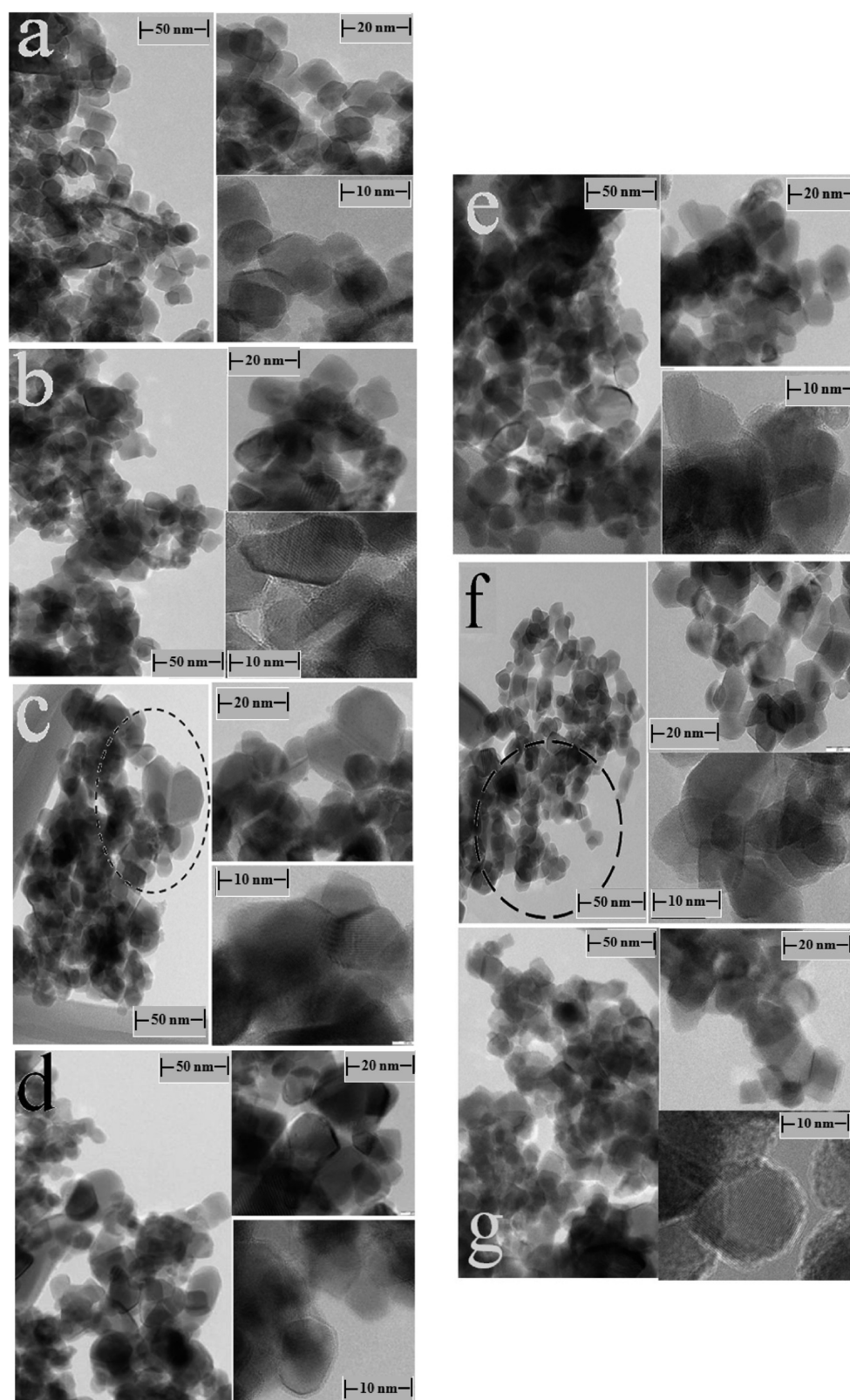


Figure 7. HRTEM micrographs of Cu:Ni/TiO₂ photocatalysts at different magnification: (a) 9Cu:1Ni-200-a, (b) 5Cu:5Ni-200-a, (c) 1Cu:9Ni-200-a, (d) 10Cu:0Ni-200-a, (e) 0Cu:10Ni-200-a, (f) bare TiO₂, and (g) 1Cu:9Ni-200-b.

lower band gap values (2.80, 2.9 eV), higher average pore diameters are favorable for 100% Orange II removal.

3.2.5. Point of Zero Charge (PZC). In the present study, PZC is determined by mass titration method,³⁴ which involved

measuring the pH at which further addition of solid catalyst did not change the pH of the suspension. Many attempts have been conducted to study the surface property of oxides of various metals. Surface charge of the oxide is a result of the acid–base

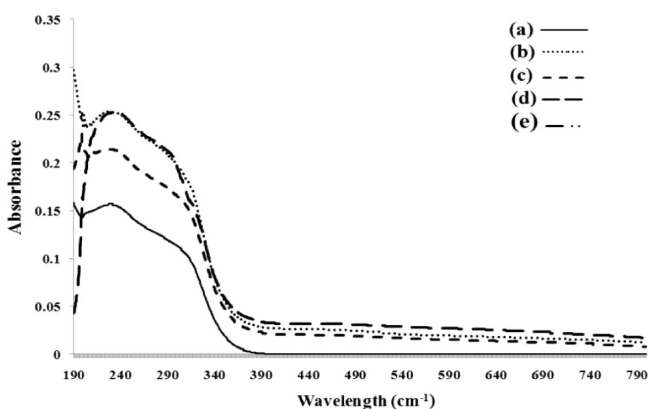


Figure 8. Absorption spectra of (a) bare TiO_2 , (b) 1Cu:9Ni-180-a, (c) 1Cu:9Ni-200-a, (d) 1Cu:9Ni-300-a, and (e) 1Cu:9Ni-200-b.

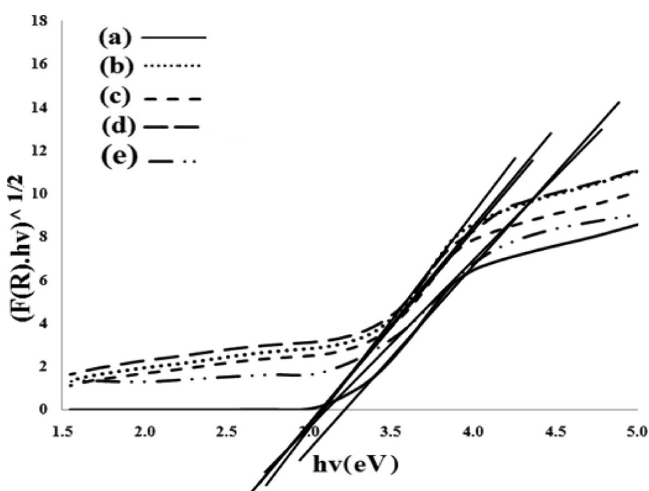


Figure 9. Plot of transformed Kubelka–Munk functions $[F(R) \cdot h\nu]^{1/2}$ versus $h\nu$: (a) bare TiO_2 , (b) 1Cu:9Ni-180-a, (c) 1Cu:9Ni-200-a, (d) 1Cu:9Ni-300-a, and (e) 1Cu:9Ni-200-b.

Table 1. Calculated Band Gap Energies and Surface Area of Bare TiO_2 and Cu–Ni/ TiO_2 Photocatalyst

photocatalyst	BET surface area (m^2/g)	total pore volume ($1/\text{cm}^3 \cdot \text{g}$)	average pore diameter (nm)	band gap energy, eV	% Orange II removal
bare TiO_2	43.1	0.20	18.5	3.16	21
1Cu:9Ni-180-a	50.0	0.32	24.8	2.90	100
1Cu:9Ni-200-a	40.0	0.30	30.1	2.80	100
1Cu:9Ni-300-a	45.8	0.33	28.2	3.19	42.0
1Cu:9Ni-200-b	53.8	0.49	18.4	2.90	65.1

equilibrium. It is a function of pH and ionic strength of the solution. It is necessary to determine the property of the photocatalysts–solution interface as the research on the photocatalyst is intended for the degradation of dyes in aqueous solution. It can be seen that with increasing photocatalyst loading, the PZC values decreased for TiO_2 (PZC = 3.8), but increased for 1Cu:9Ni-200-a (PZC = 8.8). The PZC for bare TiO_2 was acidic, which was comparable to those reported values (3.5–6.5) in the literature for TiO_2 .⁵⁸ From the results displayed in Figure 11, it can be seen that

the loading of metal oxides onto TiO_2 surface can remarkably affect the PZC values, as the PZC value increased with increasing photocatalyst loading (w/v). Results were in agreement with the work done by Di Poala et al.,^{34,59} in that the incorporation of Cu, Fe, and Co metals onto TiO_2 can increase the PZC value. In addition, if the pH of the suspension during reaction is lower than PZC, the surface charge is positive. On the other hand, if pH during reaction is higher than PZC, the surface charge is negative.³⁴ The alkaline PZC value of the Cu–Ni/ TiO_2 photocatalysts (PZC = 8.8) in the present study led to better adsorption of azo dye and its degradation as compared to the acidic surface of TiO_2 that was reported with lower performance.

3.2.6. Temperature Programmed Reduction (TPR). TPR was employed to characterize the Cu–Ni/ TiO_2 photocatalyst with respect to the type of metal oxide species present, either copper oxide, nickel oxide, or copper–nickel mixed oxide, and the degree of interaction of the oxides with TiO_2 support.³⁰ Figure 12 shows the reduction profile of 1Cu:9Ni-200-a and the monometallics 10Cu:0Ni-200-a (Cu/ TiO_2) and 0Cu:10Ni-200-a (Ni/ TiO_2). The reduction profiles clearly distinguish the reduction peaks for CuO in 10Cu:0Ni-200-a (411, 579, and 773 °C) and NiO in 0Cu:10Ni-200-a (311, 345, and 448 °C). The reduction bands at 345 and 448 °C corresponded to well-dispersed NiO with weak and strong metal–support interaction,²⁹ respectively.

The reduction profiles of 1Cu:9Ni calcined at different calcination temperatures, 180, 200, and 300, displayed quite a few reduction peaks as shown in Figure 13. For photocatalysts calcined at 180 °C, one dominant reduction peak was observed at 314 °C. Reduction peak at 314 °C might be attributed to the reduction of Cu–Ni mixed oxide instead of individual oxide. The reduction profile of 1Cu:9Ni-200-a showed one dominant peak at 270 °C and a shoulder at 240 °C. Shoulders with lower reduction temperature indicate the reduction of small CuO species having less interaction with the support. Calcination at 300 °C produced photocatalysts with one broad reduction peak at 396 °C indicating agglomeration of the particles. A clear attribution of all of the reduction peaks is complicated as there can be present more than one CuO–NiO phases on Ni-rich samples. It has been reported previously for Ni-based photocatalysts that the low reduction peak was attributed to the reduction of the NiO/CuO particles weakly interacting with the support, while the high temperature ones are assigned to the reduction of NiO (and also CuO) species in intimate contact with the support.⁶⁰ Therefore, the species that could be present at higher reduction temperature around 270–320 °C may be due to the bulk CuO^{61–63} (and NiO) having strong metal–support interaction (SMSI).^{64,65}

3.3. Orange II Removal. Ten weight % Cu–Ni/ TiO_2 photocatalysts with different Cu:Ni mass composition, calcination temperature, and preparation temperature were screened for their performance in Orange II removal. The results obtained are tabulated in Table 2 in the Supporting Information. The overall performance of metal incorporated photocatalysts was better as compared to TiO_2 (21.0% Orange II removal). Photolysis of Orange II was able to contribute to 3.0% removal. On the basis of Orange II degradation studies, photocatalyst 1Cu:9Ni-200-a, which was prepared at lower temperature (8–10 °C), displayed 100% Orange II removal, while that prepared at higher temperature (25 °C), 1Cu:9Ni-200-b, gave only 65.1% Orange II removal. Therefore, lower preparation temperature was preferred.

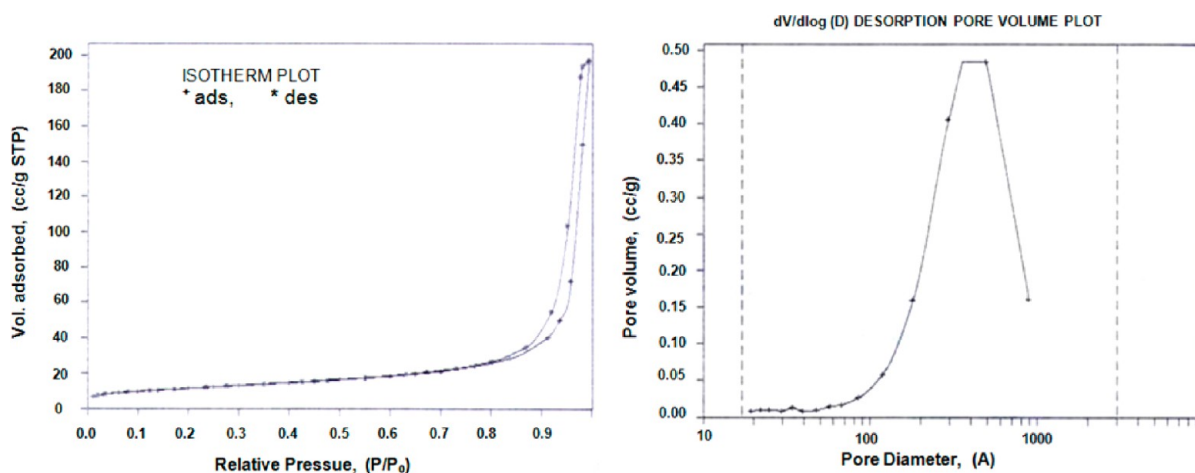


Figure 10. Isotherm plot and pore size distribution of 1Cu:9Ni-200-a.

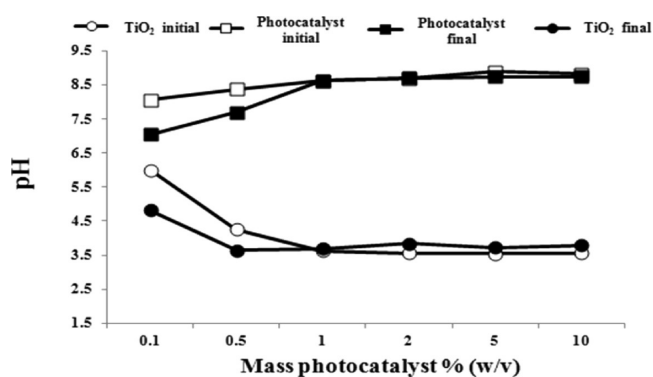


Figure 11. Plot of pH versus mass of (1Cu:9Ni-200-a) photocatalysts % (w/v).

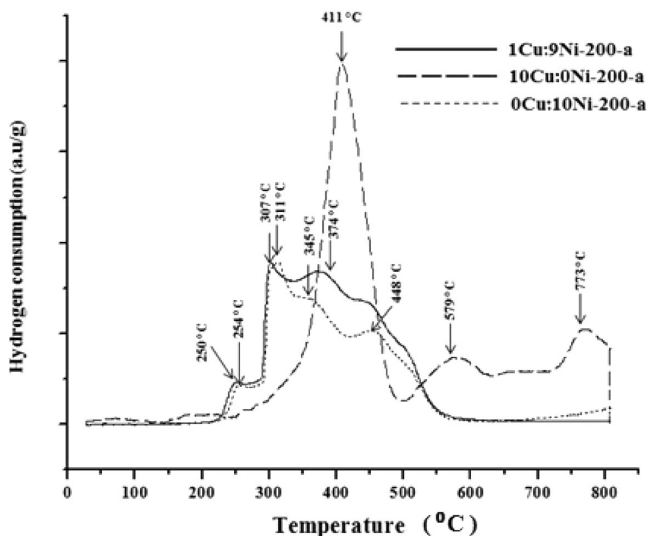


Figure 12. The TPR profiles of 1Cu:9Ni-200-a and monometallic photocatalysts.

3.3.1. Effect of Calcination Temperature. For photocatalyst with 9:1 Cu:Ni mass composition, dye removal activity was the highest (97.0%) when calcined at 180 °C as compared to that at 200 and 300 °C, which displayed 93.6% and 35.3% Orange II removal, respectively. When the Cu:Ni mass composition increased to 5:5, the optimum calcination temperature was 200

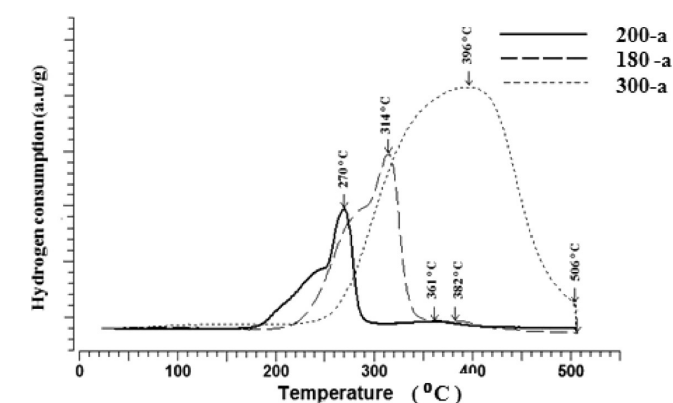


Figure 13. The TPR profiles of 1Cu:9Ni photocatalysts calcined at different temperatures.

°C, giving 88.9% Orange II removal. As the Cu:Ni mass composition increased further to 1:9, 100% Orange II removal was observed for photocatalysts calcined at both 180 and 200 °C. Higher calcination temperature at 300 °C was not desirable, giving only 42.3% Orange II removal. Photocatalysts calcined at 200 °C showed comparatively better results for dye removal for different Cu:Ni mass compositions.

3.3.2. Effect of Cu:Ni Mass Composition. It was found that the adsorption of dye onto TiO₂ depends on the electrical charge of the dye, the surface charges of the metal oxides, and the pH of a system. Azo dye like Orange II is known to adsorb onto the TiO₂ surface from the aqueous solutions.⁶⁶ The strong dependency of the capacity of TiO₂ (toward Orange II adsorption) on the pH of the solution can be explained by taking into account the PZC values of the photocatalyst. In the present study, the PZC for Cu–Ni/TiO₂ was 8.8, while the solution pH was 6.8. It was observed that the optimal solution pH was 6–7 for photocatalytic degradation of azo dyes and a decrease in activity was observed when solution was acidic or basic.⁶⁷ It was expected that when solution pH (pH 6.8) was lower than the PZC of the photocatalyst (8.8), attractive forces between the TiO₂ surface (negatively charged) and the dye (positively charged) will favor adsorption.

Orange II photolysis (3.0%) was negligible and did not result in any measurable degradation, indicating that the presence of photocatalyst was important for Orange II removal. The active material is TiO₂, and the bimetallic Cu–Ni acts as modifier to

reduce the band gap of TiO_2 .⁵⁷ The monometallic photocatalysts, 10Cu:0Ni-200-a and 0Cu:10Ni-200-a, displayed 40.4% and 56.4% Orange II removal, respectively. It can be concluded that the decolorization process is photoinduced and the fastest degradation is achieved by using visible light radiation⁶⁸ with the complete disappearance of Orange II after about 60 min of irradiation for bimetallic photocatalysts.

3.3.3. Effect of Irradiation Time. It is evident that the percentage of decolorization and photodegradation increases with irradiation time. Figure 14 displayed the absorbance

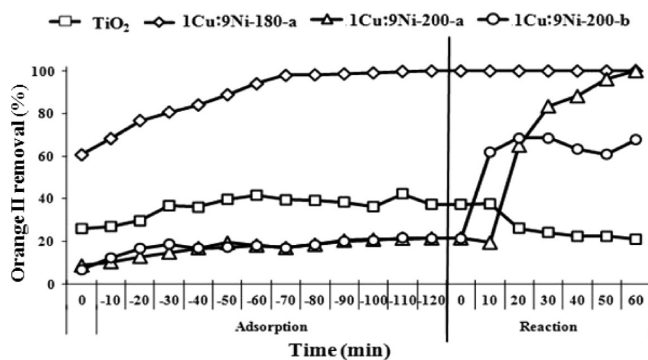


Figure 14. Effect of adsorption and irradiation time on % Orange II degradation.

spectra for Orange II degradation as a function of time (120 min dark reaction followed by 60 min light reaction) for photocatalysts with 1:9 Cu:Ni mass composition. For 1Cu:9Ni-180-a photocatalyst, decolorization was very fast (100%) and was achieved during dark reaction as compared to 1Cu:9Ni-200-a (21.3%), 1Cu:9Ni-200-b (21.3%), and TiO_2 (37.3%). For 1Cu:9Ni-200-a and 1Cu:9Ni-200-b photocatalysts, adsorption was almost similar after 120 min in the dark. Upon irradiation for 60 min, the degradation progressed further to 100% for 1Cu:9Ni-200-a photocatalyst. However, for 1Cu:9Ni-200-b and bare TiO_2 , the degradation rate was very slow, 65.1% and 21.0%, respectively.

3.4. Orange II Mineralization and Evolution of Organic Intermediates and Byproducts. In terms of dye mineralization (decomposition or oxidation of the chemical compounds), only the photocatalysts with 1:9 Cu:Ni mass composition calcined at different temperatures were investigated. Final TOC concentrations for 1Cu:9Ni-180-a, 1Cu:9Ni-200-a, and 1Cu:9Ni-300-a were 14.6, 17.3, and 31.8 ppm, respectively, as compared to the initial TOC concentration (15.87, 37.35, and 56.69 ppm). The photocatalysts calcined at 180 and 200 °C showed better results for Orange II removal and mineralization as compared to that calcined at 300 °C. From the results obtained, it is very clear that the presence of bimetallic Cu–Ni displayed a synergistic effect for dye removal. Results with improved activity for TiO_2 doped with Cu and Ni were reported for Cu–Ni/ TiO_2 ⁵⁰ for hydrogen production with respect to the monometallic ones.

It is known that complete decolorization of Orange II does not mean that the dye is completely oxidized.⁶⁹ Figure 15 corresponds to the mineralization of Orange II by photocatalytic degradation using Cu–Ni/ TiO_2 calcined at different calcination temperatures. Results are in agreement with the results reported by Kiriakidou et al.,⁶⁸ when azo dyes were mineralized using photocatalysts. Photocatalyst 1Cu:9Ni-200-a displayed 53.6% TOC removal after 60 min of irradiation, while

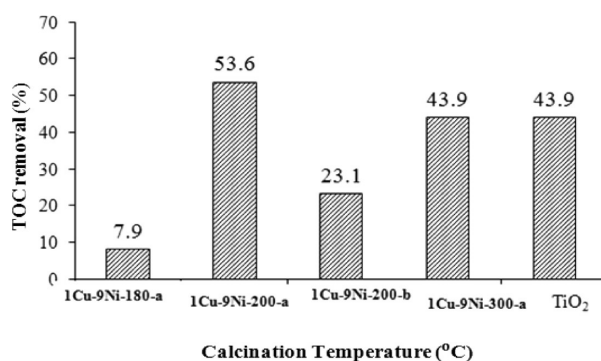


Figure 15. Effect of calcination temperature on TOC removal (%) in 1 h.

1Cu:9Ni-200-b displayed only 23.1% TOC removal. For photocatalysts 9Cu:1Ni-180-a, although decolorization was rapid (even during dark reaction), only 7.9% TOC was removed in 60 min of irradiation time. This was due to the fact that the intermediate products from Orange II degradation such as carboxyl acids are more difficult to oxidize. Therefore, complete mineralization proceeds at a much slower reaction rate⁶⁹ in which longer irradiation time is required to achieve 100% TOC removal.

To understand and clarify the changes in molecular and structural characteristics of Orange II due to photodegradation using 1Cu:9Ni-200-a under visible light irradiation, representative UV–visible spectral changes in the dye solution as a function of irradiation time were observed, and the corresponding spectra are shown in Figure 16. It can be observed from UV–vis spectra at different time interval that the absorption spectrum of Orange II in aqueous system is characterized by one main band in the visible region, with its maximum absorption at 485 nm, and by the other band in the ultraviolet region located at 310 nm. The peak at 310 nm was associated with “benzene-like” structures in the molecule, and that at 485 nm originated from an extended chromophore, comprising both aromatic rings, connected through the azo bond. The absorbance peak at 485 nm was used as the representative peak for Orange II concentration.^{35,36,68} After 40 min of irradiation time and onward, the disappearance of the visible band was observed, which might be due to the fragmentation of the azo links by oxidation.⁷⁰ In addition to this rapid decolorization effect, the decay of the absorbance at 310 nm was considered as evidence of aromatic fragment in the dye molecule and its intermediates.⁶⁸

Photodegradation intermediates and products produced during the irradiation process under visible light were identified by HPLC. Photocatalytic degradation of Orange II was reported with the evolution of different organic intermediates at different retention time during the 60 min of irradiation time. The identified intermediates were oxalic acid at RT = 1.2 min, formic acid at RT = 1.4 min, and sulfanilic acid at RT = 1.8 min. Organic intermediate at 1.8 min was also observed by Bras et al.,³⁹ who confirmed that the Orange II decolorization process was due mainly to azo bond reduction. The plot of changing concentrations of the identified organic intermediates is shown in Figure 17.

4. CONCLUSION

Bimetallic Cu–Ni/ TiO_2 photocatalysts were prepared at different temperatures with different Cu:Ni mass compositions

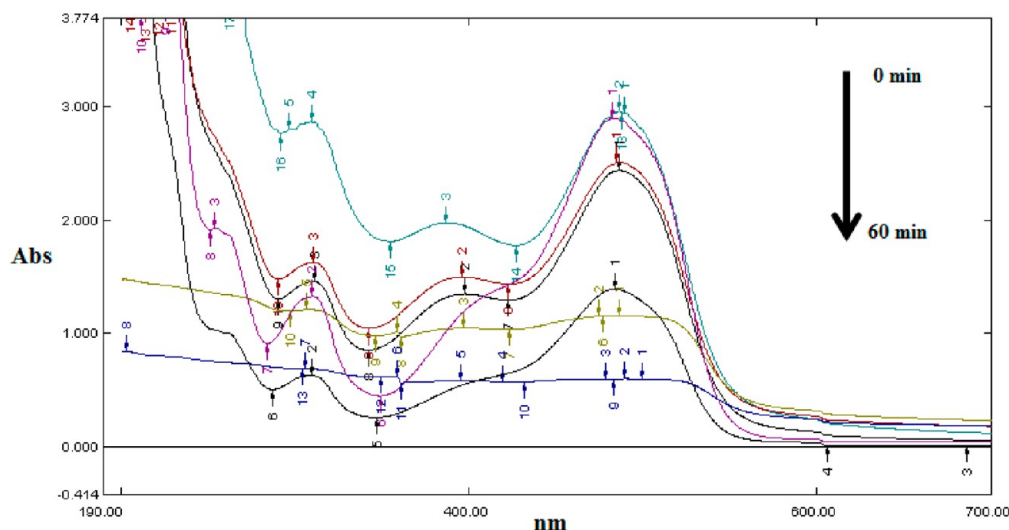


Figure 16. UV-vis spectra changes with reaction time for Orange II degradation (0–60 min).

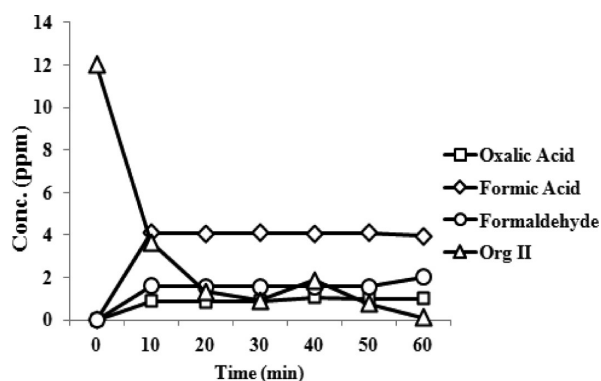


Figure 17. Intensity changes in concentration of the Orange II and degradation intermediates.

and after that calcined at different temperatures. The XRD patterns of the bimetallic photocatalysts did not show the presence of Cu or Ni phases. This is mainly due to the high metal dispersion of the metals onto TiO_2 . Results from the XRD, FESEM-EDX mapping, and HRTEM analyses were in favor to the metal particles existing in the form of well-dispersed oxides on TiO_2 surface. The surface area of photocatalysts was almost similar to that of the bare TiO_2 ($\sim 43 \text{ m}^2/\text{g}$) except for 1Cu:9Ni-200-b, which had a higher BET surface area ($53.8 \text{ m}^2 \text{ g}^{-1}$).

The photocatalyst performance of the bimetallic system is promising as compared to bare TiO_2 and the monometallic photocatalysts. In terms of preparation temperature, 1Cu:9Ni-200-a photocatalyst (prepared at 8–10 °C) displayed 100% Orange II removal as compared to 1Cu:9Ni-200-b (prepared at 25 °C) with 65.1% Orange II removal. Decolorization was the fastest for 1Cu:9Ni-180-a as compared to other photocatalysts calcined at higher temperature, which may be due to more adsorption by the increased surface area and pore volume. Although the results from UV-vis spectra showed the disappearance of the visible band with 100% Orange II removal, the TOC removal was 7.9% as compared to 1Cu:9Ni-200-a, which gave 53.6% TOC removal. Longer irradiation time is required to obtain 100% TOC removal. The identified intermediates were oxalic acid, formic acid, and salfanilic acid, where the concentration of formic acid was the

highest as compared to other identified organic intermediates. In the present work, 1Cu:9Ni-200-a was identified as the best performing photocatalyst, which displayed 100% Orange II removal (53.6% TOC removal), as compared to bare TiO_2 , which displayed only 21.0% Orange II removal (43.9% TOC removal).

■ ASSOCIATED CONTENT

📄 Supporting Information

Table of photocatalytic activity of Cu:Ni/ TiO_2 photocatalyst. This material is available free of charge via the Internet at <http://pubs.acs.org>.

■ AUTHOR INFORMATION

Corresponding Author

*E-mail: nadiariazz@gmail.com, chongfaikait@petronas.com.my.

Notes

The authors declare no competing financial interest.

■ ACKNOWLEDGMENTS

We would like to acknowledge the UTP graduate assistantship scheme for the funding to support this research work.

■ REFERENCES

- (1) Carneiro, P. A.; Osugi, M. E.; Sene, J. J.; Anderson, M. A.; Zanoni, M. V. B. Evaluation of color removal and degradation of a reactive textile azo dye on nanoporous TiO_2 thin-film electrodes. *Electrochim. Acta* **2004**, *49*, 3807–3820.
- (2) Maguire, R. J. Occurrence and persistence of dyes in Canadian river. *Water Sci. Technol.* **1992**, *26*, 265–270.
- (3) Meric, S.; Kaptan, D.; Olmez, T. Color and COD removal from wastewater containing Reactive Black 5 using Fenton's oxidation process. *Chemosphere* **2004**, *54*, 435–441.
- (4) Carliell, C. M.; Barclay, S. J.; Buckley, C. A. *Microbial Decolorization of a Reactive Azo Dye under Anaerobic Conditions*; 863; Water Research Commission: South Africa, 1995; pp 61–69.
- (5) O'Neill, C.; Hawkes, F. R.; Hawkes, D. L.; Lourenco, N. D.; Pinheiro, H. M.; Delee, W. ChemInform abstract: Color in textile effluents – Sources, measurement, discharge consents and simulation. *ChemInform* **2000**.

- (6) Rajaguru, P.; Kalaiselvi, K.; Palanivel, M.; Subburam, V. Biodegradation of azo dyes in a sequential anaerobic-aerobic system. *Appl. Microbiol. Biotechnol.* **2000**, *54*, 268–273.
- (7) Reife, A.; Freeman, H. *Environmental Chemistry of Dyes and Pigments*; Wiley/Interscience: New York, 1996.
- (8) Hoffmann, M. R.; Martin, S. T.; Choi, W.; Bahnemann, D. W. Environmental applications of semiconductor photocatalysis. *Chem. Rev.* **1995**, *95*, 69–96.
- (9) Halmann, M. *Photodegradation of Water Pollutants*; CRC Press: Boca Raton, FL, 1996; p 301.
- (10) Lachheb, H.; Puzenat, E.; Houas, A.; Ksibi, M.; Elaloui, E.; Guillard, C.; Herrmann, J.-M. Photocatalytic degradation of various types of dyes (Alizarin S, Crocein Orange G, Methyl Red, Congo Red, Methylene Blue) in water by UV-irradiated titania. *Appl. Catal., B: Environ.* **2002**, *39*, 75–90.
- (11) Chen, L.-C.; Huang, C.-M.; Tsai, F.-R. Characterization and photocatalytic activity of K⁺-doped TiO₂ photocatalysts. *J. Mol. Catal. A: Chem.* **2007**, *265*, 133–140.
- (12) Carp, O.; Huisman, C. L.; Reller, A. Photoinduced reactivity of titanium dioxide. *Prog. Solid State Chem.* **2004**, *32*, 33–117.
- (13) Fujishima, A.; Rao, T. N.; Tryk, D. A. Titanium dioxide photocatalysis. *J. Photochem. Photobiol., C* **2000**, *1*, 1–21.
- (14) Anpo, M.; Takeuchi, M. The design and development of highly reactive titanium oxide photocatalysts operating under visible light irradiation. *J. Catal.* **2003**, *216*, 505–516.
- (15) Zhang, D. Visible light-induced photocatalysis through surface plasmon excitation of platinum-metallized titania for photocatalytic bleaching of rhodamine B. *Monatsh. Chem.* **2012**, *143*, 729–738.
- (16) Zhang, D.; Zeng, F. Structural, photochemical and photocatalytic properties of zirconium oxide doped TiO₂ nanocrystallites. *Appl. Surf. Sci.* **2010**, *257*, 867–871.
- (17) Mills, A.; Le Hunte, S. An overview of semiconductor photocatalysis. *J. Photochem. Photobiol., A* **1997**, *108*, 1–35.
- (18) Ollis, D. F.; Al-Ekabi, H. *Photocatalytic Purification and Treatment of Water and Air*; Elsevier: Amsterdam, 1993.
- (19) Herrmann, J.-M. Heterogeneous photocatalysis: an emerging discipline involving multiphase systems. *Catal. Today* **1995**, *24*, 157–164.
- (20) Liu, Y.; Liu, D. Study of bimetallic Cu-Ni/ γ -Al₂O₃ catalysts for carbon dioxide hydrogenation. *Int. J. Hydrogen Energy* **1999**, *24*, 351–354.
- (21) Huang, T.-J.; Jhao, S.-Y. Ni-Cu/samarium-doped ceria catalysts for steam reforming of methane in the presence of carbon dioxide. *Appl. Catal., A: Gen.* **2006**, *302*, 325–332.
- (22) Gandarias, I.; Requies, J.; Arias, P. L.; Armbruster, U.; Martin, A. Liquid-phase glycerol hydrogenolysis by formic acid over Ni-Cu/Al₂O₃ catalysts. *J. Catal.* **2012**, *290*, 79–89.
- (23) Lázaro, M. J.; Echegoyen, Y.; Suelves, I.; Palacios, J. M.; Moliner, R. Decomposition of methane over Ni-SiO₂ and Ni-Cu-SiO₂ catalysts: Effect of catalyst preparation method. *Appl. Catal., A: Gen.* **2007**, *329*, 22–29.
- (24) Gao, W.; Jin, R.; Chen, J.; Guan, X.; Zeng, H.; Zhang, F.; Guan, N. Titania-supported bimetallic catalysts for photocatalytic reduction of nitrate. *Catal. Today* **2004**, *90*, 331–336.
- (25) Zhang, D.; Zeng, F. Photocatalytic oxidation of organic dyes with visible-light-driven codoped TiO₂ photocatalysts. *Russ. J. Phys. Chem. A* **2011**, *85*, 1077–1083.
- (26) Zhang, D. Chemical synthesis of Ni/TiO₂ nanophotocatalyst for UV/visible light assisted degradation of organic dye in aqueous solution. *J. Sol-Gel Sci. Technol.* **2011**, *58*, 312–318.
- (27) Zhang, D. Enhanced photocatalytic activity for titanium dioxide by co-modification with copper and iron. *Transition Met. Chem.* **2010**, *35*, 933–938.
- (28) Wong, R. S. K.; Feng, J.; Hu, X.; Yue, P. L. Discoloration and mineralization of non-biodegradable azo dye Orange II by copper-doped TiO₂ nanocatalysts. *J. Environ. Sci. Health, Part A: Toxic/Hazard. Subst. Environ. Eng.* **2004**, *39*, 2583–2595.
- (29) Riaz, N.; Chong, F. K.; Dutta, B. K.; Man, Z. B.; Khan, M. S.; Nurlaela, E. Photodegradation of Orange II under visible light using Cu-Ni/TiO₂: Effect of calcination temperature. *Chem. Eng. J.* **2012**, *185–186*, 108–119.
- (30) Yoong, L. S.; Chong, F. K.; Dutta, B. K. Development of copper-doped TiO₂ photocatalyst for hydrogen production under visible light. *Energy* **2009**, *34*, 1652–1661.
- (31) Marugan, J.; Christensen, P.; Egerton, T.; Purnama, H. Influence of the synthesis pH on the properties and activity of sol-gel TiO₂ photocatalysts. *Int. J. Photoenergy* **2008**, *7*.
- (32) Crouse, K. A.; Badri, M.; Hassan, H. A.; Chong, F. K. *Copper-Glycerol Complex Isolation and Characterization*; PORIM International Palm Oil Congress (Chemistry & Technology), 1996; pp 233–237.
- (33) Li, J. L.; Inui, T. Characterization of precursors of methanol synthesis catalysts, copper/zinc/aluminum oxides, precipitated at different pHs and temperatures. *Appl. Catal., A: Gen.* **1996**, *137*, 105–117.
- (34) Di Paola, A.; García-López, E.; Marci, G.; Martín, C.; Palmisano, L.; Rives, V.; Maria Venezia, A. Surface characterisation of metal ions loaded TiO₂ photocatalysts: structure-activity relationship. *Appl. Catal., B: Environ.* **2004**, *48*, 223–233.
- (35) Bourikas, K.; Styliadi, M.; Kondarides, D. I.; Verykios, X. E. Adsorption of acid Orange 7 on the surface of titanium dioxide. *Langmuir* **2005**, *21*, 9222–9230.
- (36) Zhiyong, Y.; Mielczarski, E.; Mielczarski, J.; Laub, D.; Buffat, P.; Klehm, U.; Albers, P.; Lee, K.; Kulik, A.; Kiwi-Minsker, L.; Renken, A.; Kiwi, J. Preparation, stabilization and characterization of TiO₂ on thin polyethylene films (LDPE). Photocatalytic applications. *Water Res.* **2007**, *41*, 862–874.
- (37) Konstantinou, I. K.; Albanis, T. A. TiO₂-assisted photocatalytic degradation of azo dyes in aqueous solution: kinetic and mechanistic investigations: A review. *Appl. Catal., B: Environ.* **2004**, *49*, 1–14.
- (38) Velegraki, T.; Poullos, I.; Charalabaki, M.; Kalogerakis, N.; Samaras, P.; Mantzavinou, D. Photocatalytic and sonolytic oxidation of acid Orange 7 in aqueous solution. *Appl. Catal., B: Environ.* **2006**, *62*, 159–168.
- (39) Brás, R.; Gomes, A.; Ferra, M. I. A.; Pinheiro, H. M.; Gonçalves, I. C. Monoazo and diazo dye decolourisation studies in a methanogenic UASB reactor. *J. Biotechnol.* **2005**, *115*, 57–66.
- (40) Li, G.; Qu, J.; Zhang, X.; Liu, H.; Liu, H. Electrochemically assisted photocatalytic degradation of Orange II: Influence of initial pH values. *J. Mol. Catal. A: Chem.* **2006**, *259*, 238–244.
- (41) Yan, X.; He, J.; Evans, D. G.; Zhu, Y.; Duan, X. Preparation, characterization and photocatalytic activity of TiO₂ formed from a mesoporous precursor. *J. Porous Mater.* **2004**, *11*, 131–139.
- (42) GrHfth, G. W. Quantitation of silanol in silicones by FTIR spectroscopy. *Ind. Eng. Chem. Prod. Res. Dev.* **1984**, *23*, 590–593.
- (43) Connell, G.; Dumesic, J. A. The generation of Brønsted and Lewis acid sites on the surface of silica by addition of dopant cations. *J. Catal.* **1987**, *105*, 285–298.
- (44) Bauer, A.; Lee, K.; Song, C.; Xie, Y.; Zhang, J.; Hui, R. Pt nanoparticles deposited on TiO₂ based nanofibers: Electrochemical stability and oxygen reduction activity. *J. Power Sources* **2010**, *195*, 3105–3110.
- (45) Sreethawong, T.; Suzuki, Y.; Yoshikawa, S. Photocatalytic evolution of hydrogen over mesoporous TiO₂ supported NiO photocatalyst prepared by single-step sol-gel process with surfactant template. *Int. J. Hydrogen Energy* **2005**, *30*, 1053–1062.
- (46) Zhu, H.; Wu, Y.; Zhao, X.; Wan, H.; Yang, L.; Hong, J.; Yu, Q.; Dong, L.; Chen, Y.; Jian, C.; Wei, J.; Xu, P. Influence of impregnation times on the dispersion of CuO on anatase. *J. Mol. Catal. A: Chem.* **2006**, *243*, 24–30.
- (47) Riaz, N.; Chong, F. K.; Dutta, B. K.; Man, Z. B.; Khan, M. S.; Ramli, R. M. Azo dye degradation using Cu/TiO₂ under visible light: Effect of metal loading. *2nd International Conference on Process Engineering and Advanced Materials (ICPEAM)*; IEEE: Kuala Lumpur, 2012; p 6.
- (48) Riaz, N.; Chong, F.; Dutta, B. K.; Man, Z. B.; Khan, M. S.; Nurlaela, E. Effect of calcination temperature on Orange II photocatalytic degradation using Cu: Ni/TiO₂ under visible light.

Third National Postgraduate Conference (NPC); IEEE: Universiti Teknologi PETRONAS (UTP), Tronoh, Malaysia, 2011; pp 1–5.

(49) Riaz, N.; Kait, C. F.; Dutta, B. K.; Khan, M. S.; Nurlaela, E. Photocatalytic degradation of Orange II using bimetallic Cu-Ni/TiO₂ photocatalysts. *International Conference on Fundamental and Applied Sciences (ICFAS2010)*; Kuala Lumpur Convention Centre, Kuala Lumpur, 15–17 June 2010, 2010; Kuala Lumpur Convention Centre, Kuala Lumpur, 2010.

(50) Nurlaela, E.; Chong, F. K.; Dutta, B. K.; Riaz, N. Bimetallic Cu-Ni/TiO₂ as photocatalyst for hydrogen production from water. *International Conference on Fundamental and Applied Sciences (ICFAS2010)*; Kuala Lumpur, Convention Center, Kuala Lumpur, 2010.

(51) Zhu, J.; Zheng, W.; He, B.; Zhang, J.; Anpo, M. Characterization of Fe-TiO₂ photocatalysts synthesized by hydrothermal method and their photocatalytic reactivity for photodegradation of XRG dye diluted in water. *J. Mol. Catal. A: Chem.* **2004**, *216*, 35–43.

(52) Li, Y.; Cai, M.; Rogers, J.; Xu, Y.; Shen, W. Glycerol-mediated synthesis of Ni and Ni/NiO core-shell nanoparticles. *Mater. Lett.* **2006**, *60*, 750–753.

(53) Szatmáry, L.; Bakardjieva, S.; Subrt, J.; Bezdicka, P.; Jirkovský, J.; Bastl, Z.; Brezová, V.; Korenko, M. Sulphur doped nanoparticles of TiO₂. *Catal. Today* **2011**, *161*, 23–28.

(54) Fuerte, M. D.; Hernández-Alonso; Maira, A. J.; Martínez-Arias, A.; Fernández-García, M.; Conesa, J. C.; Soria, J.; Munuera, G. Nanosize Ti–W mixed oxides: effect of doping level in the photocatalytic degradation of toluene using sunlight-type excitation. *J. Catal.* **2002**, *212*, 1–9.

(55) Wade, J. An investigation of TiO₂-ZnFeSO₄ nanocomposite for visible light photocatalysis. M.Sc. Thesis, University of South Florida, Tampa, FL, 2005.

(56) Rahimnejad, S.; Rahman, S. S.; Gholami, M. R. A credible role of copper oxide on structure of nanocrystalline mesoporous titanium dioxide. *J. Iran. Chem. Soc.* **2008**, *5*, 367–374.

(57) Nurlaela, E. Development of Cu-Ni/TiO₂ bimetallic catalyst for photohydrogen production under visible light illumination. Masters Thesis, Universiti Teknologi PETRONAS, Tronoh, Bandar Seri Iskandar, 2011.

(58) Jolivet, J.-P.; Henry, M.; Livage, J. *Metal Oxide Chemistry and Synthesis – From Solution to Solid State*; John Wiley & Sons Ltd.: Chichester, 2000; 321 pages.

(59) Di Paola, A.; García-López, E.; Ikeda, S.; Marci, G.; Ohtani, B.; Palmisano, L. Photocatalytic degradation of organic compounds in aqueous systems by transition metal doped polycrystalline TiO₂. *Catal. Today* **2002**, *75*, 87–93.

(60) De Rogatis, L.; Montini, T.; Lorenzut, B.; Fornasiero, P. Ni_xCu_y/Al₂O₃ based catalysts for hydrogen production. *Energy Environ. Sci.* **2008**, *1*, 501–509.

(61) Pintar, A.; Batista, J.; Hočevár, S. TPR, TPO, and TPD examinations of Cu_{0.15}Ce_{0.85}O_{2-γ} mixed oxides prepared by coprecipitation, by the sol–gel peroxide route, and by citric acid-assisted synthesis. *J. Colloid Interface Sci.* **2005**, *285*, 218–231.

(62) Boccuzzi, F.; Chiorino, A.; Martra, G.; Gargano, M.; Ravasio, N.; Carrozzini, B. Preparation, characterization, and activity of Cu/TiO₂ catalysts. I. Influence of the preparation method on the dispersion of copper in Cu/TiO₂. *J. Catal.* **1997**, *165*, 129–139.

(63) Mile, B.; Stirling, D.; Zammit, M. A. TPR studies of the effects of preparation conditions on supported nickel catalysts. *J. Mol. Catal. A: Chem.* **1990**, *62*, 179–198.

(64) Chang, F.-W.; Hsiao, T.-J.; Shih, J.-D. Hydrogenation of CO₂ over a rice husk ash supported nickel catalyst prepared by deposition–precipitation. *Ind. Eng. Chem. Res.* **1998**, *37*, 3838–3845.

(65) Larsson, P.-O.; Andersson, A.; Wallenberg, L. R.; Svensson, B. Combustion of CO and toluene; Characterisation of copper oxide supported on titania and activity comparisons with supported cobalt, iron, and manganese oxide. *J. Catal.* **1996**, *163*, 279–293.

(66) Vinodgopal, K.; Wynkoop, D. E.; Kamat, P. V. Environmental photochemistry on semiconductor surfaces: Photosensitized degrada-

tion of a textile azo dye, acid Orange 7, on TiO₂ particles using visible light. *Environ. Sci. Technol.* **1996**, *30*, 1660–1666.

(67) Poullos, I.; Tsachpinis, I. Photodegradation of the textile dye Reactive Black 5 in the presence of semiconducting oxides. *J. Chem. Technol. Biotechnol.* **1999**, *74*, 349–357.

(68) Kiriakidou, F.; Kondarides, D. I.; Verykios, X. E. The effect of operational parameters and TiO₂-doping on the photocatalytic degradation of azo-dyes. *Catal. Today* **1999**, *54*, 119–130.

(69) Ramirez, J. H.; Costa, C. A.; Madeira, L. M. Experimental design to optimize the degradation of the synthetic dye Orange II using Fenton's reagent. *Catal. Today* **2005**, *107–108*, 68–76.

(70) Zhang, H.; Zhang, Y.; Zhang, D. B. Decolorization and mineralization of CI Reactive Black 8 by Fenton and ultrasound/Fenton method. *Color. Technol.* **2007**, *123*, 101–105.